AGU PUBLICATIONS

JGR

Journal of Geophysical Research: Oceans

RESEARCH ARTICLE

10.1002/2017JC013473

Key Points:
- Diurnal forcing modulates the variations in seasonal temperature in the eastern shelf seas of China (ESSC)
- Diurnal wind explains over 80% of the variation in seasonal temperature induced by diurnal forcing in the ESSC
- A 3 h or shorter temporal interval of wind forcing can capture nearly 90% of the variation in seasonal temperature due to diurnal forcing

Supporting Information:
- Data Set S1
- Data Set S2
- Data Set S3
- Data Set S4
- Data Set S5
- Data Set S6
- Data Set S7
- Data Set S8
- Data Set S9
- Data Set S10
- Data Set S11
- Data Set S12

Correspondence to:
X. Guo,
guoxinyu@sci.ehime-u.ac.jp

Citation:
Yu, Y., Gao, H., Shi, J., Guo, X., & Liu, G. (2017). Diurnal forcing induces variations in seasonal temperature and Its rectification mechanism in the eastern shelf seas of China. *Journal of Geophysical Research: Oceans*, *122*, 9870–9888. https://doi.org/10.1002/2017JC013473

Received 19 SEP 2017
Accepted 23 NOV 2017
Accepted article online 30 NOV 2017
Published online 13 DEC 2017

Diurnal Forcing Induces Variations in Seasonal Temperature and Its Rectification Mechanism in the Eastern Shelf Seas of China

Yang Yu[1,2], Huiwang Gao[1,2], Jie Shi[1,2], Xinyu Guo[1,3], and Guangliang Liu[4]

[1]Key Lab of Marine Environmental Science and Ecology, Ministry of Education, Ocean University of China, Qingdao, China, [2]Laboratory for Marine Ecology and Environmental Science, Qingdao National Laboratory for Marine Science and Technology, Qingdao, China, [3]Center for Marine Environmental Studies, Ehime University, Matsuyama, Japan, [4]Shandong Provincial Key Laboratory of Computer Networks Shandong Computer Science Center (National Supercomputer Center in Jinan), Jinan, China

Abstract This study investigates the seasonal variation in temperature induced by diurnal forcing in the eastern shelf seas of China (ESSC) using a high-resolution Regional Ocean Modeling System model forced by the National Center for Environmental Prediction and the National Center for Atmospheric Research re-analysis data for surface fluxes with both 6 h and daily frequencies, respectively. The comparison between two experiments revealed a $\pm 0.4^{\circ}$C modification of the variation in seasonal temperature by diurnal forcing, which also increases the mixed-layer depth (MLD) in August by 26% and reduces the volume of the Yellow Sea Cold Water Mass (YSCWM) by 25%. Sensitivity experiments using different forcing variables indicated that diurnal wind can explain over 80% of the variability in seasonal temperature induced by diurnal forcing. Diurnal wind led to an increase in the net heat flux into the ocean by about 13 W/m^2 in summer and a decrease by about 15 W/m^2 in winter. Diurnal wind also generated an additional downward heat transport of 21 W/m^2 over the ESSC that contributed to variability in the mean MLD and YSCWM in August. Experiments changing the temporal interval of wind forcing suggested that the increase in the forcing temporal interval gradually enhanced the reproduction of the variability in seasonal temperature generated by diurnal wind; a 6 h wind forcing can capture 70% of this type of variability given by 1 h wind forcing, while a 3 h or shorter wind forcing can capture 90%.

1. Introduction

Diurnal variations in sea temperature depend primarily on variations of atmospheric forcing within a day (hereafter referred as to diurnal forcing) (Gentemann et al., 2009; Ward, 2006). Heating caused by strong insolation during the daytime generates a very thin "diurnal stratified layer" (Fairall et al., 1996b). Diurnal warming increases the daily mean sea surface temperature (SST) (Guemas et al., 2011; Katsaros et al., 2005) and modifies the air-sea fluxes of heat (Schiller & Godfrey, 2005; Ward, 2006), vapor (Cornillon & Stramma, 1985), and CO_2 (Kettle et al., 2009; Ward et al., 2004). The cooling process caused by air-sea heat exchange at nighttime deepens the mixed layer depth (MLD) (Price et al., 1986) and generates mixing across the thermocline (Bernie et al., 2005). It has also been reported that nocturnal cooling enhances nutrient transport between the mixed and subsurface layers, resulting in additional primary productivity in the upper ocean (McCreary et al., 2001).

Based on a view of scale dissimilarity, it was long believed that the impacts of diurnal forcing were limited to a diurnal time scale. One reason is because the diurnal temperature variability is only $\mathcal{O}(0.1^{\circ}\text{C})$. However, satellite and mooring observations after 1980s suggest a different view. In some extreme cases, the variability in diurnal temperature can reach a few degrees (Flament et al., 1994; Kawai & Wada, 2007; Merchant et al., 2008; Price et al., 1987; Stramma et al., 1986; Yokoyama et al., 1995). In addition, diurnal forcing was found to be able to affect phenomena ranging from the variability in intra-seasonal SST associated with the Madden–Julian oscillation (MJO) (Bernie et al., 2007; Li et al., 2013) to seasonal and inter-annual variabilities associated with monsoons (Webster et al., 1998), the Pacific Ocean warm pool (Clayson & Weitlich, 2005; Fasullo & Webster, 2000) and El Niño and the Southern Oscillation (ENSO) (Lau & Sui, 2010; Solomon & Jin, 2005).

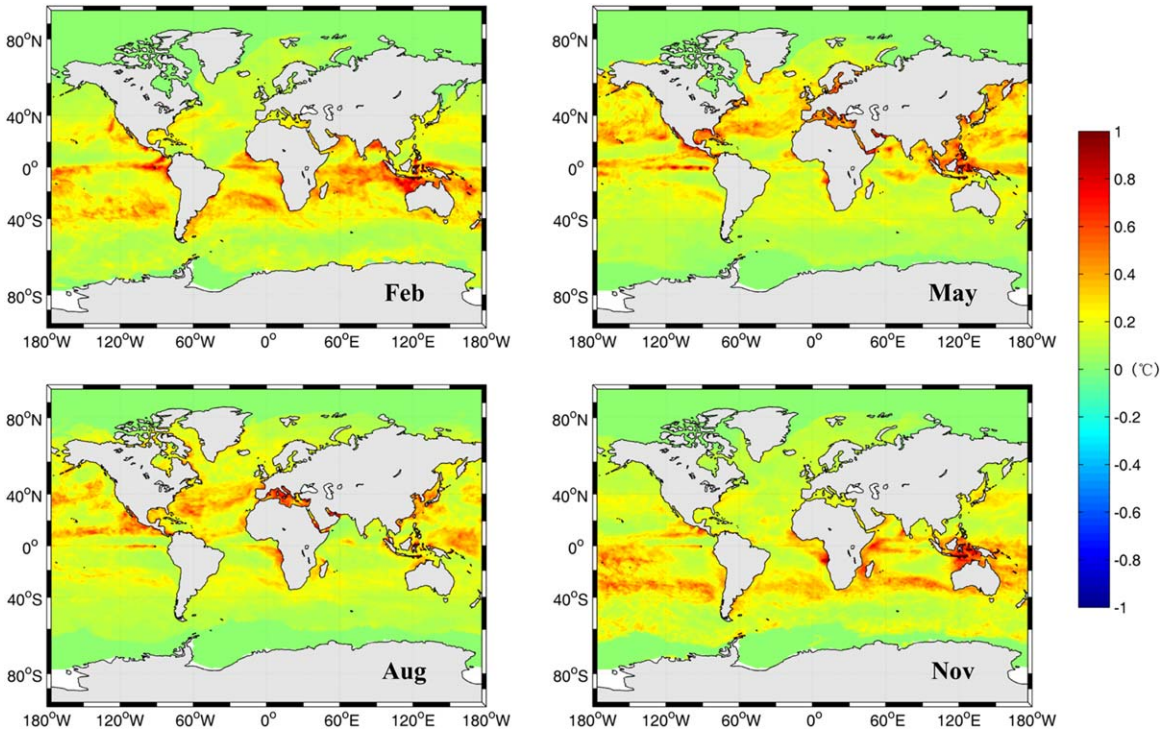

Figure 1. Monthly mean day-night difference of the Operational Sea Surface Temperature and Ice Analysis diurnal Sea Surface Temperatures (dSST) produced by an analysis of remotely sensed data acquired from March 2015–February 2016. The grid size of the SST data is 0.25°.

Variability in diurnal temperatures decreases with increasing latitude (Gille, 2012) and depth (Vialard et al., 2009) (Figure 1). For this reason, many works related to the diurnal variation in sea temperature have focused on the tropics (Kawai & Wada, 2007), where significant diurnal air-sea interaction, represented by diurnal atmospheric forcing, is essential for long-term simulations of water temperature in the tropical ocean (Zeng & Dickinson, 1998). Although variability in diurnal temperature decreases in the mid-latitudes, large variability in diurnal temperatures generated by diurnal forcing has been reported to appear seasonally in the southern Baltic Sea (Flament et al., 1994; Kahru et al., 1993) and the marginal seas around Japan and in the Sea of Okhotsk (Kawai & Kawamura, 2005; Sakaida et al., 2000). In a simulation for the global ocean, Lee and Liu (2005) demonstrated that the mid-latitude shelf sea behaves similar to the tropical seas in response to diurnal winds.

In the eastern shelf seas of China (ESSC), satellite-based diurnal temperatures derived from the global ocean Operational Sea Surface Temperature and Ice Analysis (OSTIA) system (Donlon et al., 2012) appear to vary seasonally and can approach as much as 1°C (Figure 1). A preliminary simulation study for the ESSC demonstrated that high-frequency diurnal forcing is able to induce significant variations in summertime temperatures inside the ocean (Yu et al., 2017). As a result, the mixed layer depth (MLD) increased by about 10% in summer, and the mean volume of the Yellow Sea Cold Water Mass (YSCWM) decreased by about 30%. However, Yu et al. (2017) did not provide a physical interpretation of the change in summertime temperature with diurnal forcing. Unlike the tropics, where the diurnal insolation is suggested to be the most important factor (Zeng & Dickinson, 1998), the mechanism involved in the mid-latitude shelf region is expected to be more complex (Hyder et al., 2011; Webster et al., 1996). Therefore, as an extension of the work of Yu et al. (2017), we carried out many sensitivity experiments in this study with these goals: 1) confirming the findings of Yu et al. (2017) by extending the model integration time and 2) clarifying the mechanism responsible for the seasonal variation in temperature induced by diurnal atmospheric forcing.

In this paper, sections 2–4 describe the methodology, present the results of the model experiments, and explain the mechanism for the diurnal atmospheric forcing induced seasonal variation in temperature, respectively. Sections 5 and 6 examine the sensitivity of the variation in seasonal temperature induced by

diurnal forcing to the frequency of atmospheric forcing, and provide a summary and recommendations for future research studies, respectively.

2. Methodology

In order to investigate the variation in seasonal temperature induced by diurnal forcing in the ESSC, a three-dimensional Regional Ocean Modeling System (ROMS) model (Shchepetkin & Mcwilliams, 2005) was applied in the present study. To capture additional details related to the variation in temperature, the model horizontal resolution was set to 1/18° (about 6 km) with the meridional range from 24°N to 41.3°N, and the zonal range from 117°E to 132°E (Figure 2). The model had 26 terrain-following "S"-layers in the vertical direction, and the water depth at each grid point was from a 1/60° resolution bathymetry database provided by the Laboratory for Coastal and Ocean Dynamics Studies, Sung Kyun Kwan University, Korea. The enhanced vertical resolution near the sea surface achieved by using Shchepetkin's double stretching function (Shchepetkin & Mcwilliams, 2009) ensures that the thickness of the uppermost model layer, even at the deepest water point, was less than 1 m (Bernie et al., 2005). The Mellor-Yamada level 2.5 turbulence closure

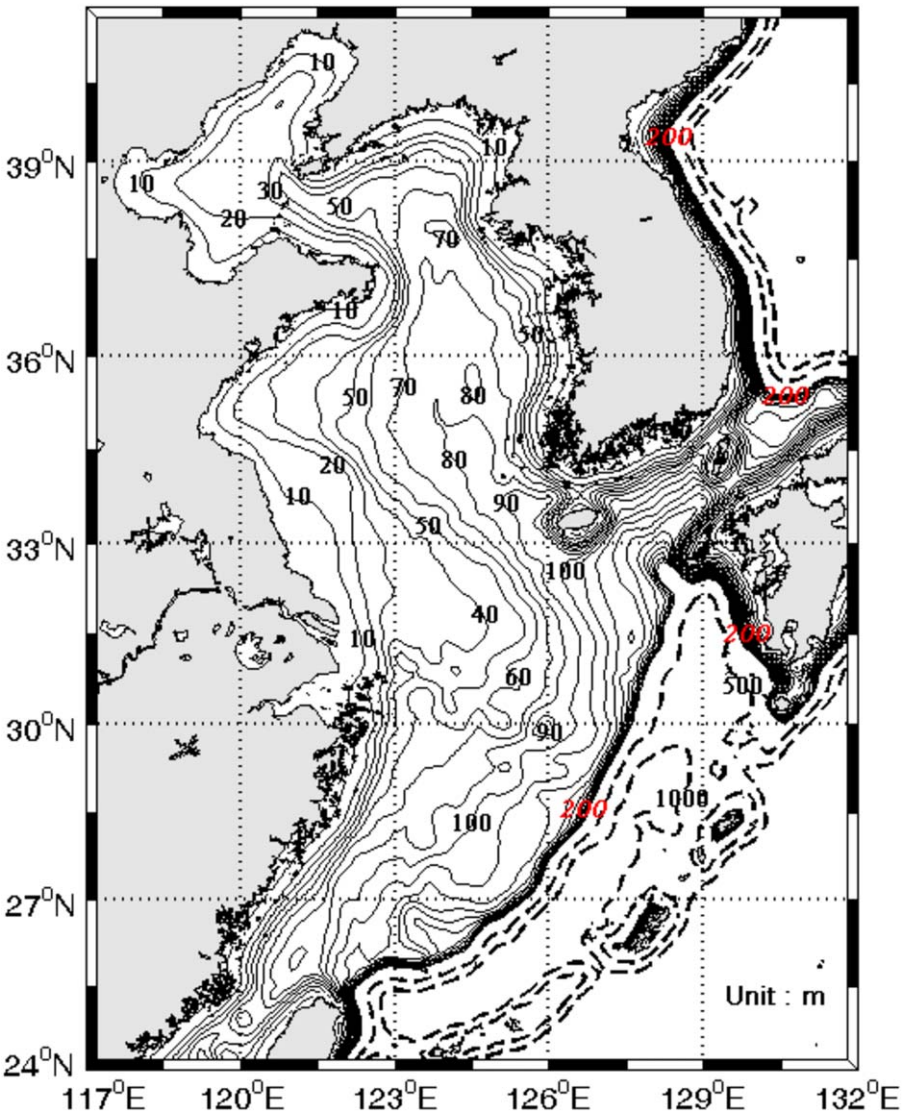

Figure 2. Model domain and bottom topography (m). The contour interval is 10 m, from 0 to 200 m. The eastern shelf seas of China in this study were defined as the area with a water depth of less than 200 m in this figure.

scheme (MY2.5) (Mellor & Yamada, 1982) was performed to represent the vertical mixing. The quadratic bottom drag coefficient for bottom stresses was set to 1.5×10^{-3}.

2.1. Initial Conditions

We used climatological data for the mean monthly temperature and salinity in January from the World Ocean Atlas 2013 data set (http://www.nodc.noaa.gov/OC5/woa13/) (Boyer et al., 2005; Locarnini et al., 2013; Zweng et al., 2013) as an initial field of the model. The initial current velocity as well as the sea surface height (SSH) in the model are from monthly mean climatological data derived from the CARTON-GIESE Simple Ocean Data version 2.2.4 data set (http://iridl.ldeo.columbia.edu/SOURCES/.CARTON-GIESE/.SODA/.v2p2p4/) (Carton & Giese, 2008; Carton et al., 2000) averaged from 1991 to 2008 for January.

2.2. Open Boundary Conditions

Ten principal tidal constituents of M_2, S_2, N_2, K_2, K_1, O_1, P_1, Q_1, M_f and M_m were specified at lateral boundaries as the high-frequency boundary conditions. Their harmonic constants of elevation and currents were derived from the Oregon State University global inverse tidal model of TPXO7.0 (http://volkov.oce.orst.edu/tides/) (Egbert & Erofeeva, 2002; Egbert et al., 1995). Mean monthly Simple Ocean Data version 2.2.4 climatological data were applied for the low-frequency boundary conditions of SSH and ocean currents, while the monthly World Ocean Atlas 2013 was used to obtain the climatological data for temperature and salinity. The Chapman type condition (Chapman, 1985) for SSH, the Flather type condition (Flather, 1976) for the barotropic velocity, and the Orlanski type radiation condition (Orlanski, 1976) for the temperature and salinity were used in the model.

2.3. River Discharge

There are ten rivers inside the model domain: the Yangtze, Yellow, Huaihe, Liaohe, Haihe, Luanhe, Minjiang, Qiantang, Yalu, and Han rivers. Data related to the mean monthly climatological discharge for these rivers were collected from the Global River Discharge Project (http://daac.ornl.gov/RIVDIS/rivdis.shtml) (Vorosmarty et al., 1998).

2.4. Atmospheric Forcing and Hindcast Simulation

Solar radiation was directly employed in the model using a double exponential absorption function (Paulson & Simpson, 1977) with Jerlov water type II parameters. The long wave radiation was calculated by the Berliand algorithm (Berliand, 1952). The wind stress, latent heat flux, and sensible heat flux were calculated by bulk formulas (Fairall et al., 1996a) with the COARE3.0 parameterization scheme (Fairall et al., 2003). The necessary SST for the calculation of latent, sensible, and long wave heat fluxes was from our ocean model. The "cool skin" effect, which significantly affects the air-sea heat exchange and generates a very thin (0.1–1 mm) thermodynamic "cool-skin layer" at the top of the ocean, was also considered in the study using the "cool skin" correction scheme given by Fairall et al. (1996b). The air pressure was also given as forcing to the ocean model.

The impacts of diurnal forcing were examined by a comparison of two experiments: the diurnal forcing case (Diurnal Case) and the daily forcing case (Daily Case) (Table 1). High-frequency (collected four times a day) data, specifically the National Center for Environmental Prediction/National Center for Atmospheric Research (NCEP/NCAR) re-analysis data (Kalnay et al., 1996), were obtained. Seven variables were used including wind speed (at 10 m above the surface), short wave radiation, air temperature (2 m), air pressure

Table 1
Temporal Interval of Atmospheric Forcing Used in Numerical Experiments

	Wind speed	Solar radiation	Air temperature	Air pressure	Precipitation rate
Daily case	Daily	Daily	Daily	Daily	Daily
Case 1	4 times a day	Daily	Daily	Daily	Daily
Case 2	Daily	4 times a day	Daily	Daily	Daily
Case 3	Daily	Daily	4 times a day	Daily	Daily
Case 4	Daily	Daily	Daily	4 times a day	Daily
Case 5	Daily	Daily	Daily	Daily	4 times a day
Diurnal case	4 times a day	4 times a day	4 times a day	4 times a day	4 times a day

(2 m), precipitation rate, cloud fraction, and relative humidity. These data were obtained from the NCEP/NCAR website (http://www.esrl.noaa.gov/psd/data/gridded/data.ncep.reanalysis.html). Because the cloud fraction and relative humidity have been known as the major error terms related to air-sea flux estimation (Gill, 1982) and are known to be important to the seasonal variation in temperature in the mid-latitudes (Webster et al., 1998), we kept their frequency at four times a day in two cases. The other five variables were given four times a day in the Diurnal Case, while their daily means were given once a day in the Daily Case (Table 1).

For a spin-up, the model was integrated for 20-years forced by the diurnal (four times a day) NCEP/NCAR forcing from 1 January 1991 to 31 December 2010. Then, the model was integrated for 5 years from 1 January 2011 to 31 December 2015 using the corresponding forcing given in Table 1. The model results in the 5 years (2011–2015) were saved with an interval of 1 h for further analysis.

3. Model Results

3.1. Modeling Diurnal and Seasonal Variations in Temperature in the ESSC

To examine whether 6 h atmospheric forcing used in the Diurnal Case is able to capture variability in the diurnal temperature in the ESSC, an hourly satellite SST data (http://marine.copernicus.eu/services-portfolio/access-to-products/?option=com_csw&view=details&product_id=SST_GLO_SST_L4_NRT_OBSERVATIONS_010_014) derived from the OSTIA system was used to check the model results. Spatially averaged hourly SSTs over the ESSC given by our model and OSTIA from March 2015 to December 2015 are shown in Figure 3. The correlation coefficient of the diurnal SST anomaly, which is defined as the difference of hourly SST from its daily mean between the Diurnal Case and the OSTIA data, was 0.74. In addition, the diurnal range of variation, defined as a positive anomaly maximum minus a negative anomaly maximum during a day, had a correlation coefficient of 0.68 for the Diurnal Case and the OSTIA data. Although a noticeable displacement existed between the Diurnal Case and the OSTIA data (Figure 3), which may be caused by the bias of the daily mean SST in the model, the model simulates the diurnal variation of SST in the ESSC very well.

The model performance for reproducing seasonal variation of water temperature was validated by a comparison with field observational data from four cruises operated by the Ocean University of China in March, July, October, and December 2011. These field observational data have been used to examine the seasonal variation of water masses in the southern Yellow Sea and the East China Sea by Quan et al. (2013). Our model simulates well the seasonal variation in temperature in the ESSC; model temperatures in both the Diurnal and Daily Cases have similar spatial distributions with the observational data at depths of 10 m (Figures 4a–4c, 4e–4g, 4i–4k, and 4m–4o) and 50 m (Figures 5a–5c, 5e–5g, 5i–5k, and 5m–5o). Model temperature bias (column mean) is less than 1°C in more than 50% the hydrological stations, especially in the Diurnal Case, where this proportion approaches 65%. On average, the model temperature (10 m) is 0.7°C higher than the observational data in the four cruises in the Diurnal Case and 1.2°C higher in the Daily Case. The Diurnal Case has a smaller Centered Root Mean Square Difference in both the upper (10 m; Figures 4d, 4h, 4l and 4p) and deeper (50 m; Figures 5d, 5h, 5l and 5p) layers than in the Daily Case. Therefore, it is likely that diurnal atmospheric forcing gives the ocean model better performance in reproducing variability in seasonal temperatures in the ESSC.

3.2. Variations in Seasonal Temperature Induced by Diurnal Forcing

The good performance of model simulation for the diurnal and seasonal variations of water temperature in the ESSC shows that the model is reasonable for investigating the variation in seasonal temperature induced by diurnal forcing. Furthermore, the better performance of reproducing variability in the seasonal temperature in the Diurnal Case than in the Daily Case (Figures 3–5) suggests that diurnal atmospheric forcing likely affects the variation in seasonal temperature in the ESSC. In order to understand the variation in seasonal temperature induced by diurnal forcing in detail, we present the difference of seasonal mean water temperature at several model layers between the Diurnal and Daily Cases (Figure 6). The seasonal mean was calculated from 5 years of model outputs with an interval of 1 h in the same season.

In the warm season (MAM and JJA), diurnal forcing produces a vertically uneven temperature bias (Figures 6e–6g and 6i–6k). The difference in the horizontally averaged temperature over the ESSC between the Diurnal and Daily Cases increased with water depth, varying from −0.4°C at the surface to 0.4°C at the

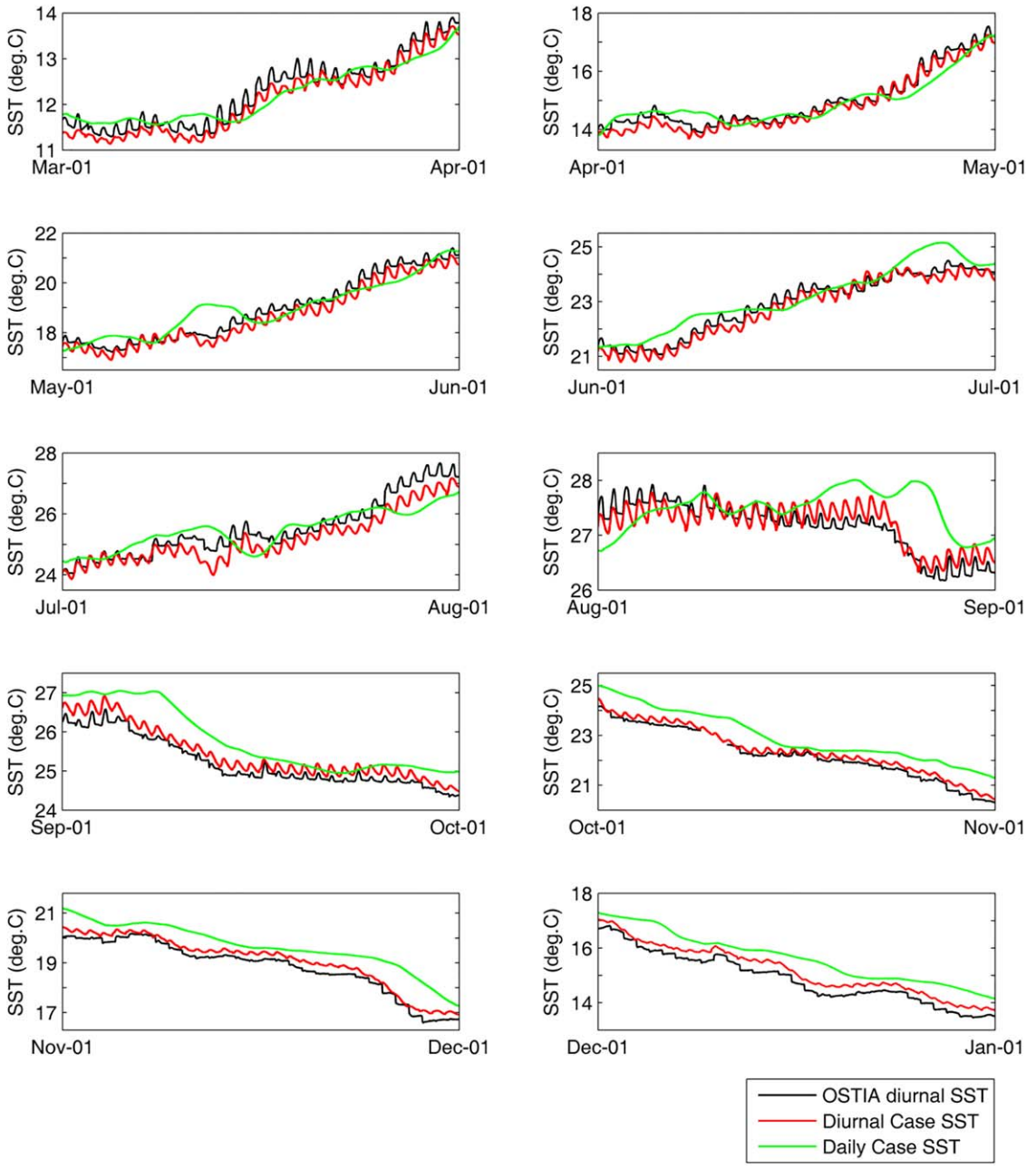

Figure 3. Time series of hourly mean area-averaged Sea Surface Temperature (SST) from March 2015 to December 2015 obtained by Daily Case (green curve), Diurnal Case (red curve) and Operational Sea Surface Temperature and Ice Analysis data (black curve) in the eastern shelf seas of China.

bottom (Figures 6h and 6l). This vertical inconsistency in horizontally-averaged temperature bias developed from spring (Figure 6h) to summer (Figure 6l), implying that diurnal forcing induces a more downward transportation of heat, which will be examined more in section 4. The negative surface temperature bias generated by diurnal forcing appears in most regions of the ESSC in the warm season (Figures 6e and 6i), but the positive bottom temperature bias occurs mainly in the Yellow and Bohai Seas (Figures 6g and 6k). In the Yellow and Bohai Seas, the bottom temperature bias induced by diurnal forcing has an order of 1°C, which is larger than the horizontally-averaged value of 0.4°C over the entire ESSC (Figure 6l), except for the coastal areas where strong tidal currents induce a well-mixed structure of temperature.

The temperature bias between the Diurnal and Daily Cases in the warm season appears in both the vertical and horizontal directions. The horizontal variation in the temperature bias is likely to be associated with

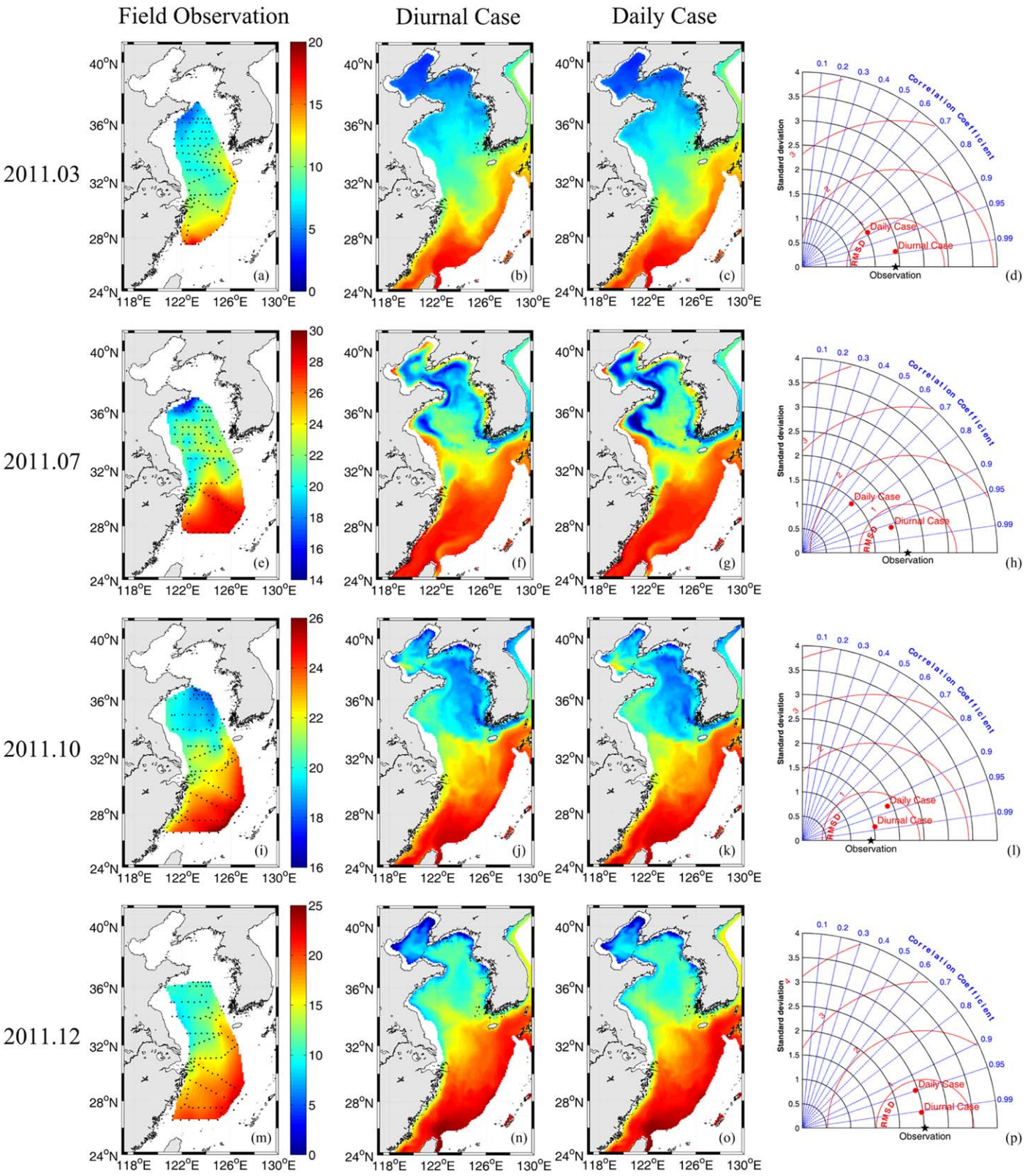

Figure 4. Distributions of temperature at a 10 m depth from (a, e, i, m) four cruises; (b, f, j, n) diurnal cases; and (c, g,k, o) daily cases. (d, h, l, p) The Taylor diagrams. Black dots in Figures 4a, 4e, 4i, and 4m are hydrographic stations. Model temperatures are time-averaged over the duration of four cruises for spatial distribution (middle two columns) but a snapshot value with the exact time was the observational data in the Taylor diagram (right column).

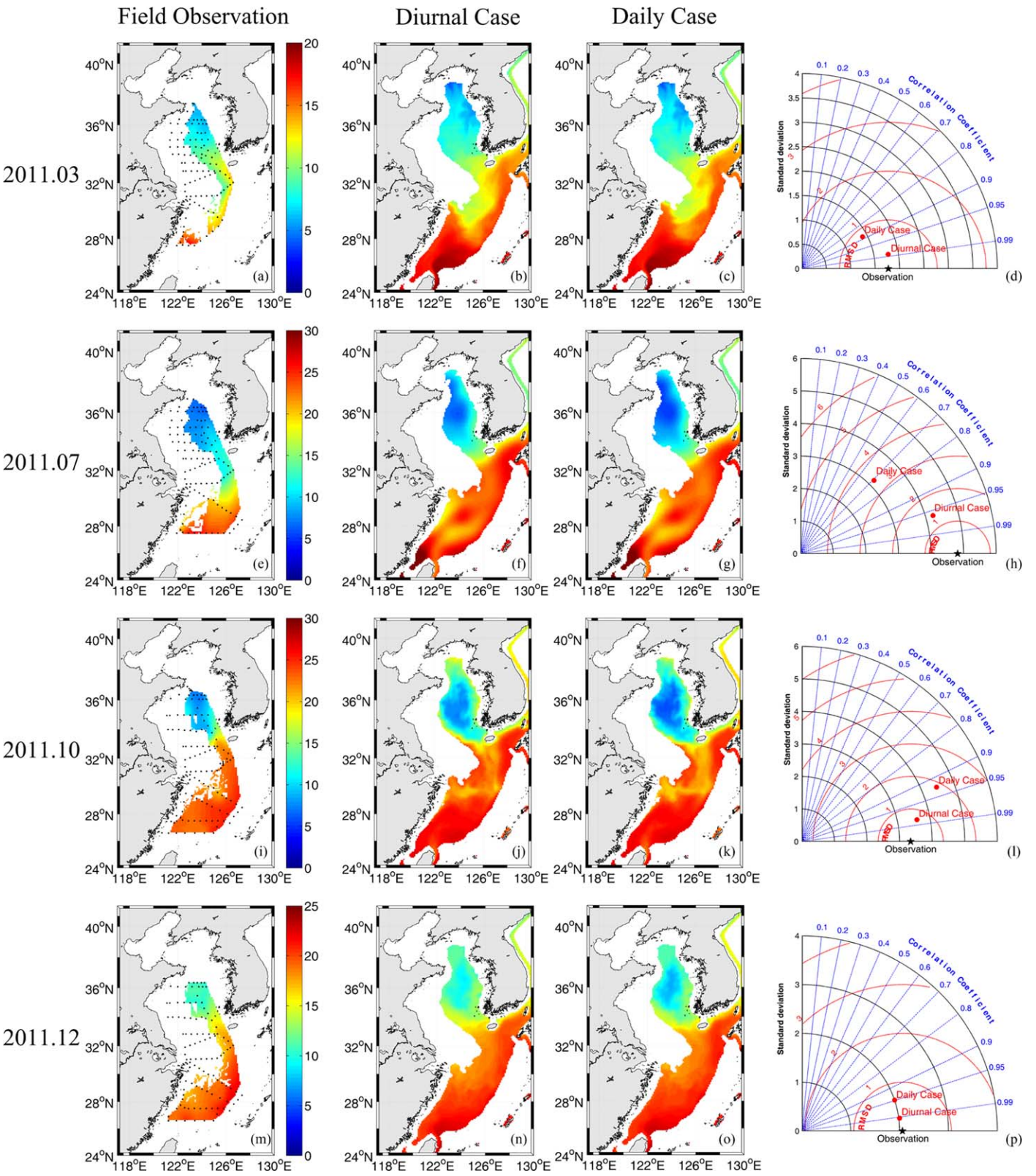

Figure 5. Same as Figure 4 except for 50 m depth.

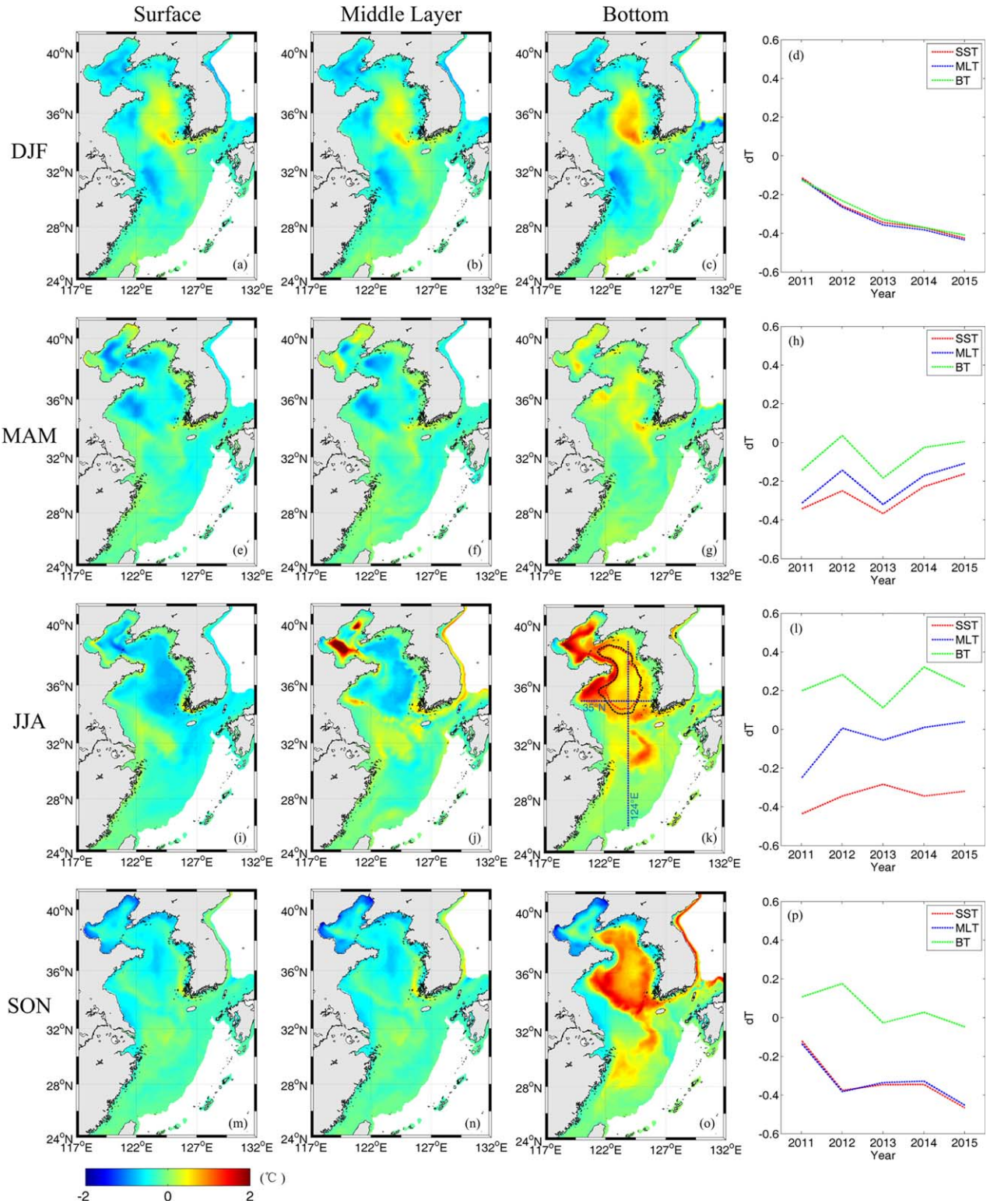

Figure 6. Seasonal mean differences of sea surface temperatures (SST). (a, e, i, m) Middle layer temperatures (MLT). (b, f, j, n) Bottom temperature (BT). (c, g, k, o) Between diurnal and daily cases. (d, h, f, p) Spatially averaged values at three layers over the eastern shelf seas of China. Because the model uses a terrain-following "S"- coordinate system, the depths of these layers change with water depth and have not a fixed depth at all grid points. As an average over the entire ESSC, the surface layer has a depth of 0 m, the middle layer has a depth of 31 m, and the bottom layer has a depth of 63 m. The areas surrounded by dotted lines in Figure 6k are the areas of Yellow Sea Cold Water Mass in the Diurnal Case (red line) and in the Daily Case (black line). The blue dashed lines in Figure 6k are positions of 35°N and 124°E sections used in Figure 9. Note: DJF, December–February; MAM, March–May; JJA, June–August; and SON, September–November.

some specific processes in the ESSC, such as in the diluted Yangtze River water and its front (Figures 6i–6k). However, the focus of this study is on the general effects of atmospheric forcing for the entire ESSC. Therefore, we will not discuss the role of a specific ocean process in the changes of water temperature with diurnal forcing in more detail.

In the cold season (SON and DJF), diurnal forcing gradually offsets the vertically inconsistent temperature bias from the surface to the bottom (Figures 6a–6c and 6m-o) and finally produces a vertically consistent negative temperature bias of −0.4 to −0.1°C (Figure 6d). Therefore, the diurnal forcing likely generates an additional cooling effect in the cold season.

Although the temperature bias induced by diurnal forcing in winter is negative for horizontally averaged temperature bias over the entire ESSC (Figure 6d), it presents a positive value (0.2–0.4°C) in the central Yellow Sea from the surface to bottom (Figures 6a–6c). This positive temperature bias in the central Yellow Sea (Figure 6c) is probably associated with the bottom-warming induced by diurnal forcing in the warm season (Figures 6g and 6k). Since the surface cooling induced by diurnal forcing in the cold season is not enough to remove the stored heat in the bottom of the central Yellow Sea in the warm season (Figures 6g, 6k, and 6p), a positive temperature bias appears there in winter (Figures 6c and 6o).

Interestingly, the vertically consistent negative temperature bias has a negative trend of −0.08°C yr^{-1} (r^2 = 0.92, P < 0.01, Figure 6d) over the 5 years of model integration. We will present the reason for this trend in section 4. Here we only note the possibility that an ocean model without diurnal forcing may overestimate the water temperature in the cold season, which could be a potential problem during climate modeling with long integration times.

3.3. Changes of Summer MLD and YSCWM

Vertically inconsistent temperature differences between the Diurnal and Daily Cases in the warm season (Figures 6h and 6l) suggest a unique influence of diurnal forcing on the variation of summertime temperatures in the ocean. Strong summer stratification usually weakens the upper ocean mixing in the mid-latitude shelf sea (Simpson & Bowers, 1981), and low-frequency forcing and ocean processes themselves are not able to capture the variability in summertime MLD (Qiao et al., 2004; Xia et al., 2006). Here we examine the influence of diurnal forcing on the variation of summertime MLD that is defined as the minimum depth of the vertical temperature gradient above 0.2°C/m (Thomson & Fine, 2003; Yu et al., 2017), which is usually at the upper bound of the seasonal thermocline in the ESSC (Wei et al., 2001). The monthly mean of spatially averaged MLD over the ESSC in August in the Diurnal and Daily Cases are listed in Table 2. The monthly mean MLD was 13.3 m in the Diurnal Case but only 10.6 m in the Daily Case. The MLD increases from Daily Case to Diurnal Case by 26% in August, which is larger than the averaged 12% increasing over the period from May to August. Therefore, the increasing range of changes in MLD is induced by diurnal forcing within a month, and the changes in August are probably effective indicators that can be used to assess the effects of diurnal forcing.

Table 2
Seasonal Amplitude of Diurnal Forcing Induced Perturbation in the Air-Sea Heat Flux (ADSH) and Mixed Layer Depth (MLD) in August, and Mean Water Temperature and Volume of Yellow Sea Cold Water Mass (YSCWM) From May to November in Different Experiments

			YSCWM	
	ADSH (W/m^2)	MLD (m)	Mean temperature (° C)	Mean volume ($\times 10^{12}$ m^3)
Daily case		10.6	8.5	4.22
Case 1	12.5	13.2	8.9	3.11
Case 2	1.5	10.7	8.5	4.17
Case 3	5.6	10. 6	8.5	4.14
Case 4	0.2	10.6	8.5	4.21
Case 5	0.4	10.6	8.5	4.22
Diurnal case	15.2	13.3	8.9	3. 12

A comparison of the Diurnal and Daily Cases shows that a large deviation occurs in the summertime bottom temperature (Figure 6k) in the central Yellow Sea that overlaps with the area of the YSCWM. The YSCWM is a bottom water mass with relatively low temperature below the strong thermocline in the central Yellow Sea from May to November and is usually bordered by a 10°C isotherm (Fei et al., 2005; Li et al., 2016; Zhang et al., 2008). The mean temperature of the YSCWM from May to November was 8.9°C in the Diurnal Case but was 8.5°C in the Daily Case (Table 2). The mean volume of the YSCWM was $3.1\times 10^{12}m^3$ in the Diurnal Case and $4.2\times10^{12}m^3$ in the Daily Case. Therefore, the diurnal atmospheric forcing increases the temperature of the YSCWM by about 0.4°C and reduces the volume of the YSCWM by about $1.1\times10^{12}m^3$, which is one quarter of the volume in the Daily Case. Since the occupied horizontal area of the YSCWM is similar in the Diurnal and Daily Cases (Figure 6k), the change in volume of the YSCWM is likely to be induced by a vertical process rather than by a horizontal one. The relationship between the changes of MLD and YSCWM will be examined in section 4.

4. Discussions

Diurnal atmospheric forcing generates a diurnal variation in water temperature (Bernie et al., 2005; Price et al., 1987) that conversely has feedback to affect the heat exchange between air and sea (Ward, 2006; Webster et al., 1996). To investigate the causes for the variation in seasonal temperature induced by diurnal forcing presented in section 3, we evaluated the air-sea heat flux generated by diurnal forcing. The diurnal forcing generates a warm bias of net heat flux into the ocean by 13 W/m^2 in summer (August) and a cold bias by -15 W/m^2 in winter (December) (Figure 7a). Consequently, the diurnal forcing activates the air-sea heat exchange and induces more heat transfer from the air into the ocean in summer and more heat out of ocean into the air in winter (Figure 7a). This seasonal heat flux generated by diurnal forcing is of the same order as that in the tropics (Webster et al., 1996).

The altered net heat flux due to diurnal forcing is caused mainly by latent heat because it varies the most among the three components of heat flux associated with diurnal forcing (Figure 7a). Sensible heat also contributes to this alteration but is a secondary factor. Long wave radiation causes a small contribution of only 2 W/m^2 to the net heat flux change. The change of long wave radiation was consistent with the 0.4°C reduction of the SST in the Diurnal Case as compared with the Daily Case. Over a time scale of one year, diurnal forcing causes the ocean to release more heat to the atmosphere, with a flux of 0.9 W/m^2. If we integrate this heat flux for a period of one year and divide it by the product of seawater heat capacity of 4.0×10^6 $J\ m^{-3}\ {}^{\circ}C^{-1}$ and the averaged water depth over the ESSC (63 m), we obtain an order of 0.1°C yr^{-1} for the temperature difference between the Diurnal and Daily Cases. Because the lateral boundary condition is almost the same for the two cases, a gradual cooling occurs in the Diurnal Case and induces a negative trend of 0.08°C yr^{-1} for temperature bias (Figure 6d).

4.1. Key Factor Contributing to Diurnal Forcing in the ESSC

The negative bias of the net heat flux from September to the next April (Figure 7a) can explain the lower temperature in the Diurnal Case than in the Daily Case for the cold season (Figures 6d and 6p). However,

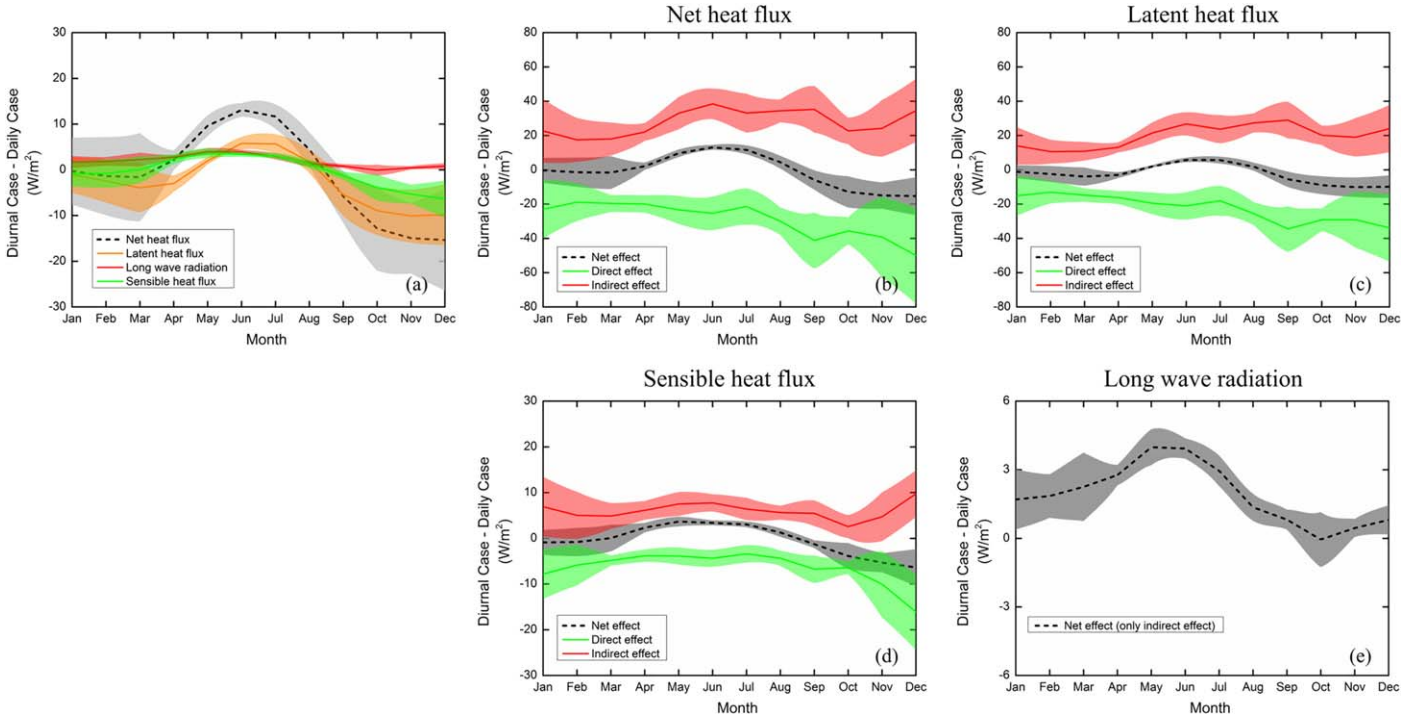

Figure 7. (a) Averages of air-sea net heat flux (dashed line), latent heat flux (orange curve), long wave radiation (red curve) and sensible heat flux (green curve) over the eastern shelf seas of China induced by diurnal forcing. The diurnal-wind-generated direct (green line), indirect (red line) and net (gray dash line) effects on air-sea heat flux in the form of (b) net, (c) latent, and (d) sensible heat fluxes and (e) long wave radiation. Values for this figure are monthly ones averaged from the same month and are the results of 5 years of simulations. The shadow in colors is the standard deviation corresponding to the monthly mean denoted by lines of the same color. Positive values indicate heat entering the ocean from the atmosphere.

the positive bias of the net heat flux from May to August (Figure 7a) does not match the lower SST in the Diurnal Case and the Daily Case for the warm season (Figures 6h and 6l). This result is different from our previous understanding from the tropics where diurnal forcing traps solar radiation energy into the "diurnal stratified layer," raising the daily mean SST, causing the ocean to release more heat to the atmosphere (Webster et al., 1996).

To clarify the mechanism for the variation in seasonal temperature induced by diurnal forcing in the ESSC, we carried out several sensitivity experiments to address the key factor in diurnal forcing. In these experiments, we changed the frequency of one atmospheric forcing variable from daily to four times a day (Table 1) and kept all the other configurations for the model run the same as were used in the Daily Case. We use three indices to evaluate the effects of changing the frequency of each atmospheric forcing parameter on the temperature change on a seasonal scale. One is the amplitude of the seasonal air-sea heat flux (ADSH) generated by diurnal forcing, defined as the range of the monthly mean difference of net heat flux between one case and the Daily Case over one year. The other two are the monthly MLD averaged over the ESSC in August and the YSCWM-related variables (temperature and volume) averaged from May to November. The ADSH was 12.5 W/m^2 in Case 1, while the MLD increased from the Daily Case to Case 1 by 2.6 m, the mean temperature of the YSCWM increased from the Daily Case to Case 1 by 0.4°C and the mean volume of the YSCWM decreased from the Daily Case to Case 1 by 1.1×10^{12} m^3 (Table 2). Compared with the values given in Table 2 for the change in the three indices from the Daily to Diurnal Case, the frequency of wind forcing, i.e., the diurnal wind, explains 82% of the increase in ADSH, 96% of the increase in MLD and almost 100% of the change in two variables related to the YSCWM. Unlike in the tropics, where diurnal insolation is the most important factor (Zeng & Dickinson, 1998), diurnal wind is the most effective factor responsible for the variation in seasonal temperature induced by diurnal forcing in the ESSC. Though the day-night differences in SST and vertical temperature profile are affected by diurnal insolation (Bernie et al., 2005), our results suggest that the diurnal variations in heat fluxes have little effects on seasonal temperature. It is the diurnal variations in wind forcing that affect the seasonal temperature in the ESSC through the modification of the daily mean surface state variables.

4.2. Direct and Indirect Effects of Diurnal Wind on Air-Sea Heat Flux

Wind speed is involved the bulk calculation of latent and sensible heat fluxes. To determine the difference in wind speed between the Daily and Diurnal Cases, Figure 8 presents the wind speed averaged over the ESSC in 2015. The measurement of wind speed at a frequency of four times a day (red line) shows apparent diurnal changes with positive and negative anomalies from the daily wind speed (green line). The daily mean wind speed (blue line), which is defined as a scalar mean of four wind speeds during a day, is different from the daily wind speed that was calculated as the magnitude of daily wind velocity, i.e., vector mean of four wind velocities during a day. The difference between the blue and green lines changes with time and probably depends on the difference between the red and green lines, which represent the magnitude of diurnal wind. Over a year, the daily mean wind speed (blue line, represented by the Diurnal Case) is underestimated by the daily wind speed (green line, represented by the Daily Case) by 0.5 m/s; this is 8% of the annual mean wind speed over the ESSC.

To understand how the diurnal wind affects the heat flux, we separated its effect into two parts. One part was caused by the underestimation of daily mean wind speed and is called the direct effect in this study. The other was caused by the change of SST and SST related to specific humidity and is called the indirect effect. In this study, the heat fluxes were calculated by following bulk equations (1)–(3):

$$Q_e=\rho_a L_e C_e S(q_w-q_a) \tag{1}$$

$$Q_h=\rho_a c_p C_h S(\theta_w-\theta_a) \tag{2}$$

$$Q_b=\epsilon\sigma_{SB}\theta_w^4\left(0.39-0.05e^{1/2}\right)\left(1-kC^2\right)+4\epsilon\sigma_{SB}\theta_w^3(\theta_w-\theta_a), \tag{3}$$

where Q_e, Q_h, and Q_b are latent heat flux, sensible heat flux, and long wave radiation, respectively; ρ_a is the air density; L_e is the latent heat of vaporization; c_p is the specific heat of air at constant pressure; ϵ is the emittance of the sea surface; σ_{SB} is Stefan-Boltzmann constant; k is the cloud cover coefficient; C is the cloud fraction; S is the wind speed at a 10-m height over the sea relative to the surface current; q is specific humidity; θ is the potential temperature; the subscripts w and a are the values at the surface and at a 2-m

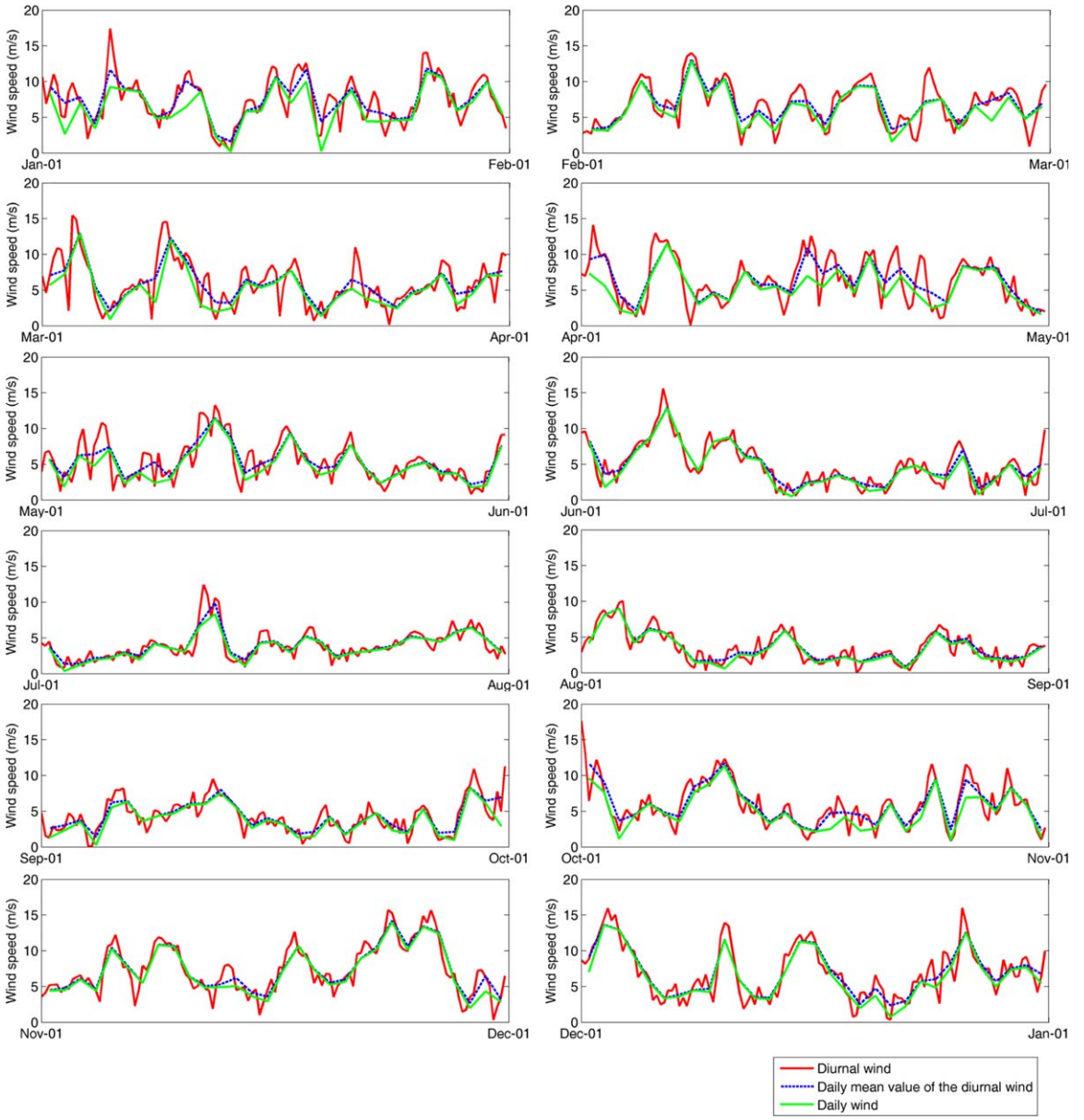

Figure 8. Spatially averaged wind speed over the eastern shelf seas of China from January to December, 2015. The red, blue, and green lines are the 6 h wind speed, the daily mean of the 6 h wind speed, and the daily wind speed, respectively, obtained as the magnitude of daily wind velocity.

height over the sea, respectively; and C_e and C_h are the turbulent exchange coefficients for moisture and heat, respectively.

The changes of the net heat flux and its four components from the Daily Case to Case 1 can be written using equations (4)–(8):

$$dQ_n = dQ_s + dQ_e + dQ_l + dQ_b \tag{4}$$

$$dQ_s = 0 \tag{5}$$

$$dQ_e = \frac{\partial Q_e}{\partial S} dS + \frac{\partial Q_e}{\partial q_w} \frac{\partial q_w}{\partial \theta_w} d\theta_w \tag{6}$$

$$dQ_h = \frac{\partial Q_h}{\partial S} dS + \frac{\partial Q_h}{\partial \theta_w} d\theta_w \tag{7}$$

$$dQ_b = \frac{\partial Q_b}{\partial \theta_w} d\theta_w, \tag{8}$$

where Q_n and Q_s are the net heat flux and short wave radiation, respectively.

Equations (4)–(8) divide the diurnal-wind-generated heat flux (dQ_n) into the direct (terms including change of wind speed, dS) and indirect effects (terms including change of SST, $d\theta_w$). Latent and sensible heat fluxes (Figures 7c and 7d) include direct and indirect effects, while long wave radiation (Figure 7e) includes only indirect effects. Regrouping equations (4)–(8), the direct and indirect effects of diurnal wind on the net heat flux can be evaluated by equations (9) and (10):

$$Direct\ \ effect = \left(\frac{\partial Q_e}{\partial S} + \frac{\partial Q_h}{\partial S}\right) dS \tag{9}$$

$$Indirect\ \ effect = \left(\frac{\partial Q_e}{\partial q_w}\frac{\partial q_w}{\partial \theta_w} + \frac{\partial Q_h}{\partial \theta_w} + \frac{\partial Q_b}{\partial \theta_w}\right) d\theta_w. \tag{10}$$

The similarity between Figures 7a and 7b (broken grey lines) indicates that the separation of the direct and indirect effects of diurnal wind can explain the seasonal air-sea heat flux induced by diurnal forcing over the ESSC. The direct effects cause the ocean to release additional heat into the atmosphere with a value of 19–45 W/m^2, and the indirect effects enhance the absorption of heat by the ocean at 15–35 W/m^2 (Figure 7b). The two effects are in a competitive relationship. In winter (December), the direct effects are larger than the indirect effects and cause the ESSC to release additional heat into atmosphere with a flux of 15 W/m^2. In summer (August), the indirect effects are larger than the direct effects and cause the ESSC to absorb more heat from the atmosphere with a flux of 13 W/m^2. As an annual mean, these two effects cause the ESSC to release more heat to the atmosphere with a flux of 0.9 W/m^2.

4.3. High- and Low-Frequency Influences on Air-Sea Heat Flux

Besides the separation of direct and indirect effects, the role of diurnal wind can also be understood from its frequency. Here we define the high-frequency effect as the change in heat flux caused by diurnal variation in the wind speed and the associated diurnal variation in SST, and the low-frequency effect as that caused by the difference of daily mean SST and wind speed between the Daily Case and Case 1. To quantify high- and low-frequency effects of diurnal wind, we decompose the wind speed, SST, and surface specific humidity (q_w) using equations (11)–(13):

$$S = \langle S \rangle + S^* \tag{11}$$

$$\theta_w = \langle \theta_w \rangle + \theta_w^* \tag{12}$$

$$q_w = \langle q_w \rangle + q_w^*, \tag{13}$$

where $\langle \cdot \rangle$ denotes the daily mean value, and the asterisk denotes the diurnal signal.

Substituting equations (11)–(13) into equations (1)–(3), respectively, we get:

$$Q_e(S, q_w) = Q_e(\langle S \rangle, \langle q_w \rangle) + Q_e\left(\langle S \rangle, q_w^*\right) + Q_e(S^*, \langle q_w \rangle) + Q_e\left(S^*, q_w^*\right) - Q_e(\langle S \rangle, 0) - Q_e(S^*, 0) \tag{14}$$

$$Q_h(S, \theta_w) = Q_h(\langle S \rangle, \langle \theta_w \rangle) + Q_h\left(\langle S \rangle, \theta_w^*\right) + Q_h(S^*, \langle \theta_w \rangle) + Q_h\left(S^*, \theta_w^*\right) - Q_h(\langle S \rangle, 0) - Q_h(S^*, 0) \tag{15}$$

$$Q_b(\theta_w) = Q_b(\langle \theta_w \rangle) + Q_b\left(\theta_w^*\right) + \left(Q_b(\theta_w) - Q_b(\langle \theta_w \rangle) - Q_b\left(\theta_w^*\right)\right). \tag{16}$$

In the above decomposition, the parameters such as L_e, C_e and C_h are calculated using the original value θ_w.

Equations (14)–(16) divide the air-sea heat fluxes into three parts: the terms involving daily mean values including $Q_e(\langle S \rangle, \langle q_w \rangle)$, $-Q_e(\langle S \rangle, 0)$, $Q_h(\langle S \rangle, \langle \theta_w \rangle)$, $-Q_h(\langle S \rangle, 0)$ and $Q_b(\langle \theta_w \rangle)$; the terms involving diurnal signals including $Q_e\left(S^*, q_w^*\right)$, $-Q_e(S^*, 0)$, $Q_h\left(S^*, \theta_w^*\right)$, $-Q_h(S^*, 0)$, and $Q_b\left(\theta_w^*\right)$; and the others involving both daily mean values and diurnal signals. We calculated all the terms in equations (14)–(16) using the results of Daily Case and Case 1, and this creates a spatial average for the difference in these terms between two cases in summer (August) and winter (December) (Table 3).

Table 3
High-Frequency (Diurnal) and Low-Frequency (Daily Mean) Influences of Diurnal Wind on the Seasonal Air-Sea Heat Flux in the Eastern Shelf Seas of China[a,b]

Winter (December)					
$Q_e(\langle S\rangle, \langle q_w\rangle)$	$Q_e(\langle S\rangle, q_w^*)$	$Q_e(S^*, \langle q_w\rangle)$	$Q_e(S^*, q_w^*)$	$-Q_e(\langle S\rangle, 0)$	$-Q_e(S^*, 0)$
−10.0	8.9	0.1	-0.1	-8.9	0.1
$Q_h(\langle S\rangle, \langle \theta_w\rangle)$	$Q_h(\langle S\rangle, \theta_w^*)$	$Q_h(S^*, \langle \theta_w\rangle)$	$Q_h(S^*, \theta_w^*)$	$-Q_h(\langle S\rangle, 0)$	$-Q_h(S^*, 0)$
−5.7	5.2	0.1	-0.1	-5.2	0.1
$Q_b(\langle \theta_w\rangle)$	$Q_b(\theta_w^*)$	$Q_b(\theta_w) - Q_b(\langle \theta_w\rangle) - Q_b(\theta_w^*)$			
1.0	-0.2	0.2			
Summer (August)					
$Q_e(\langle S\rangle, \langle q_w\rangle)$	$Q_e(\langle S\rangle, q_w^*)$	$Q_e(S^*, \langle q_w\rangle)$	$Q_e(S^*, q_w^*)$	$-Q_e(\langle S\rangle, 0)$	$-Q_e(S^*, 0)$
5.2	18.3	0	0.1	-18.3	-0.1
$Q_h(\langle S\rangle, \langle \theta_w\rangle)$	$Q_h(\langle S\rangle, \theta_w^*)$	$Q_h(S^*, \langle \theta_w\rangle)$	$Q_h(S^*, \theta_w^*)$	$-Q_h(\langle S\rangle, 0)$	$-Q_h(S^*, 0)$
3.2	11.7	0	0.1	-11.7	-0.1
$Q_b(\langle \theta_w\rangle)$	$Q_b(\theta_w^*)$	$Q_b(\theta_w) - Q_b(\langle \theta_w\rangle) - Q_b(\theta_w^*)$			
4.0	0	0			

[a]Monthly mean difference between daily case and case 1.
[b]Unit is W/m^2.

The terms involving daily mean values ($Q_e(\langle S\rangle, \langle q_w\rangle)$, $-Q_e(\langle S\rangle, 0)$, $Q_h(\langle S\rangle, \langle \theta_w\rangle)$, $-Q_h(\langle S\rangle, 0)$, $Q_b(\langle \theta_w\rangle)$) and the terms $Q_e(\langle S\rangle, \theta_w^*)$ and $Q_h(\langle S\rangle, \theta_w^*)$ present relatively large differences between the Daily Case and Case 1. Among these terms, $Q_e(\langle S\rangle, \theta_w^*)$, and $Q_h(\langle S\rangle, \theta_w^*)$ can be balanced by $-Q_e(\langle S\rangle, 0)$ and $-Q_h(\langle S\rangle, 0)$, respectively (Table 3). Consequently, only the terms of $Q_e(\langle S\rangle, \langle q_w\rangle)$, $Q_h(\langle S\rangle, \langle \theta_w\rangle)$ and $Q_b(\langle \theta_w\rangle)$ really affect the seasonal air-sea heat flux over the ESSC.

The important three terms in Table 3 involve the difference of daily mean wind speed, SST, and specific humidity between the Daily Case and Case 1. Such a difference is caused directly by the diurnal wind used in Case 1. The results given in Table 3 indicate that the linkage between diurnal wind and heat flux is acted on by the daily mean values of some state variables. Therefore, the correction for heat flux using observational SST (Barnier et al., 1995) is really helpful to increase the accuracy of air-sea heat flux in the calculations without diurnal forcing.

4.4. Intensified Downward Heat Transport by Diurnal Wind in Summer

Diurnal wind not only modulates seasonal heat exchange at the sea surface but also generates a downward heat transport in the ocean in summer (Figures 6h and 6l). To understand its spatial structure, we presented the monthly mean temperature in August along sections 124°E and 35°N in the Daily Case and Case 1 (Figure 9). The model results present a strong summer thermocline in the ESSC, and this thermocline is deeper in Case 1 than in the Daily Case (Figures 9a–9d). Water temperature above the thermocline is lower in Case 1 than in the Daily Case (Figures 9e and 9f), but the temperatures at and below the thermocline were higher in Case 1 than in the Daily Case (Figures 9e and 9f). This finding suggests that an apparent summertime downward heat transport was generated by diurnal wind.

To quantify the downward heat transport caused by diurnal wind, we calculated the difference in heat content and horizontal transport (horizontal advection and diffusion) at each grid point for the Daily Case and Case 1, respectively. This difference corresponds to the amount of vertical heat transport. Integrating the calculated vertical heat transport for the grid points where the mean water temperature in August was lower in Case 1 than in the Daily Case (see the area above the red line in Figures 9e and 9f as an example), we obtained the difference in vertical heat transport (5.97×10^{19} J) for the ESSC between two cases. This indicates that an additional downward heat transport of 21 W/m^2 existed over the ESSC in August and was caused by the diurnal wind. This vertical heat transport resulted in a decrease of the mean temperature in the upper mixed layer of 0.4°C (Figures 9e and 9f), explaining the lower SST that was observed in the Diurnal Case than in the Daily Case (Figure 6l). Eighty-four percent of this vertical heat transport (about 5.03×10^{19} J) was trapped by the seasonal thermocline, whose mean temperature in August increased by 3°C (Figures 9e and 9f). Consequently, the depth of the thermocline increased by 2.1 m (Figures 9a–9d), and the mean MLD increased by 2.6 m from the Daily Case to Case 1 (Table 2). The increase of the depth of the seasonal thermocline in Case 1 also explains the reduction of YSCWM volume by 1.1×10^{12} m^3 in summer

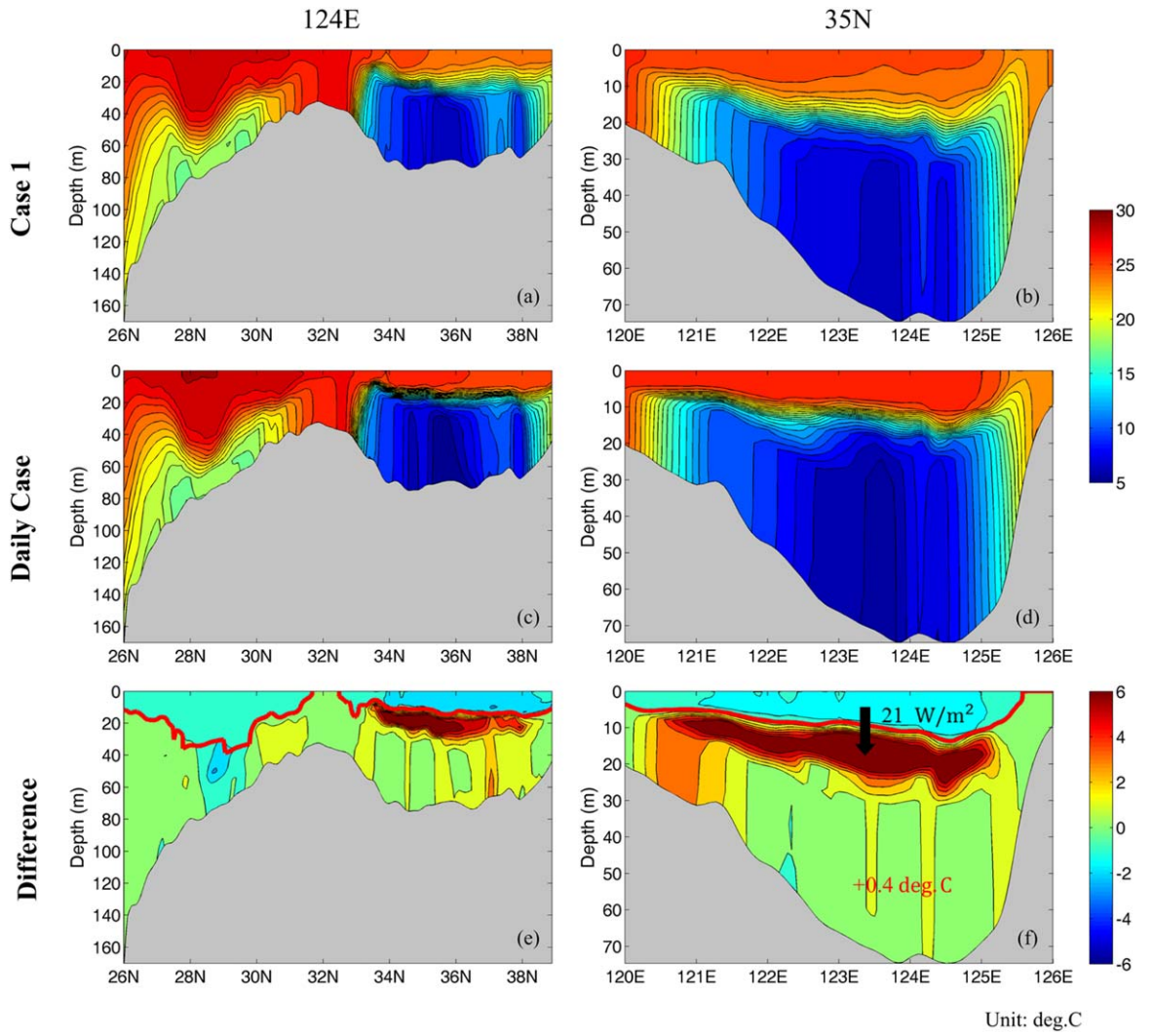

Figure 9. Monthly mean temperature along 35°N and 124°E sections (whose positions are shown in Figure 6k) in August. (a), (b) Case 1; (c), (d) Daily Case; and (e), (f) the differences between Case 1 and the Daily Case. Red lines in Figure 9e and f show the interface for calculation of vertical heat transport.

(Table 2). The remaining 9.36×10^{18} J of vertical heat transport, which refused the restraint of the thermocline, found its way into the layer deeper than the thermocline. Half of it, about 4.41×10^{18} J, contributed to a 1°C increase in water temperature in the Yellow and Bohai Seas (Figures 6k and 9e). The other, about 4.95×10^{18} J, contributed to a 0.4°C increase in the mean temperature in the YSCWM in Case 1 (Figure 9f and Table 2).

5. Sensitivity to the Wind Forcing Frequency

In the tropics, where the diurnal insolation dominates the longer time-scale variability in temperature that is induced by diurnal forcing, a 3 h or better temporal resolution of heat fluxes is required to capture 90% of the variability in diurnal SST and 95% of the intra-seasonal variability in SST (Bernie et al., 2005). In the ESSC, diurnal wind is the most effective factor affecting the variation in seasonal temperature induced by diurnal forcing. To examine the sensitivity of the variation in seasonal temperature with the frequency of wind, additional experiments were carried out with wind forcing from the NCEP Climate Forecast System (CFS-R/CFSv2; http://apdrc.soest.hawaii.edu/data/data.php) (Saha et al., 2010) at a variety of temporal resolutions (1 h, 3 h, 6 h, 12 h, and 24 h; Figure 10). The variability in seasonal temperature generated by diurnal wind are assumed to be fully resolved by 1 h wind forcing (100%) and fully unresolved by 24 h wind forcing

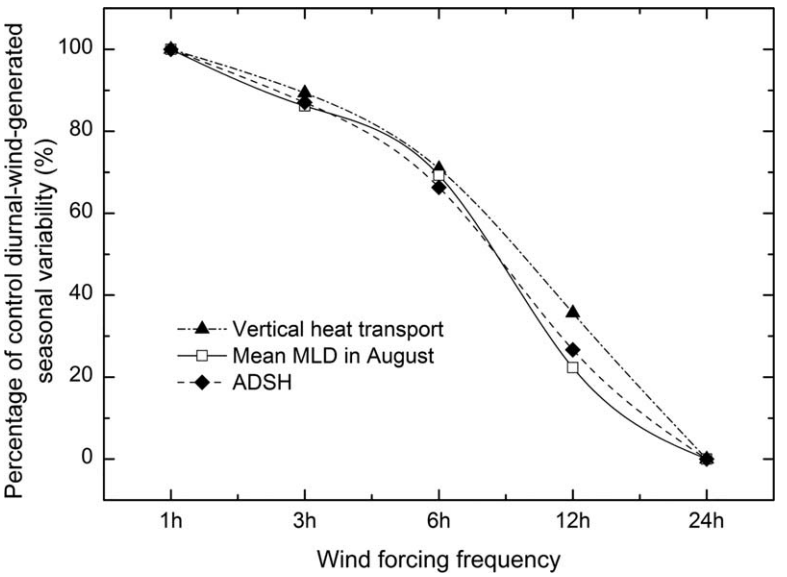

Figure 10. Reproduced percentage of the variation in seasonal temperature generated by diurnal wind in the eastern shelf seas of China by the wind forcing with different time intervals. The dotted line represents the diurnal-wind-generated vertical heat transport in August; the solid line represents the diurnal-wind-increased mean mid layer depth (MLD) in August; the dashed line represents air-sea heat flux (ADSH).

(0%). Except for wind forcing, these experiments used the same configurations as the Diurnal Case and were integrated for a period of 5 years from 1 January 2011 to 31 December 2015.

The 6 h wind forcing caused the model to reproduce 66% of the ADSH, 69% of the mean MLD increased by diurnal wind in August, and 71% of the vertical heat transport generated by diurnal wind in August (Figure 10). Being similar to the conclusion of Bernie et al. (2005) for the tropics, a 3 h or better temporal resolution of wind forcing is necessary for reproducing 90% of the variation in seasonal temperature generated by diurnal wind in the ESSC.

6. Conclusions

Diurnal atmospheric forcing affects the seasonal variation in temperature in the ESSC. Diurnal forcing generates a seasonal temperature variability of $\pm 0.4^{\circ}C$ and enhances the heat by the ocean in summer with a surface heat flux of 13 W/m^2 and the release of ocean heat in winter with a surface heat flux of 15 W/m^2. Diurnal forcing intensifies the downward transportation of heat in summer and increases the mean MLD by 26% in August. The enhanced summertime ocean heat absorption and downward heat transport affects the YSCWM, raising its temperature by 0.4°C and reducing its volume by 25%.

Wind is the most effective variable among the specified variables with a diurnal frequency. Diurnal wind explains over 80% of the variation in seasonal temperature induced by diurnal forcing in the ESSC. These winds account for about 8% of the magnitude of the increase in the daily mean wind speed (about 0.5 m/s) in the ESSC and hence modify the daily mean SST. The daily mean wind speed and SST, as modified by diurnal wind, generate direct and indirect effects on the seasonal air-sea heat flux. Diurnal wind also generates an additional downward heat transport of 5.97×10^{19} J inside the ocean in August that is equivalent to 21 W/m^2, explaining the variation in summertime temperature induced by diurnal forcing in the ESSC.

High-frequency wind is probably important for the simulation of seasonal temperatures in the ESSC because a 3 h or better temporal resolution of wind forcing is necessary to reproduce 90% of the seasonal variation in temperature generated by diurnal wind. This may be taken as an important reference for simulations of seasonal temperature in the mid-latitude oceanic shelf region. The results of the present study imply that the air-sea coupling simulation needs a time-step of at least less than 3 h for the exchange of momentum and heat flux between the air and sea.

Acknowledgments
We are grateful for support from the National Key Basic Research Program of China (grant 2014CB953700) and the NSFC - Shandong Joint Fund for Marine Ecology and Environmental Sciences (U1606404). X. Guo thanks the Fundamental Research Funds for Central Universities from the Ministry of Education of China (201512004) and the Grant-in-Aid for Scientific Research on Innovative Areas (MEXT KAKENHI grant: JP15H05821) for support. We thank two anonymous reviewers for their helpful comments. The data for all the figures and tables are provided as the supporting information to the manuscript and the full data set is available by contacting the corresponding author.

References

Barnier, B., Siefridt, L., & Marchesiello, P. (1995). Thermal forcing for a global ocean circulation model using a three-year climatology of ECMWF analyses. *Journal of Marine Systems*, *6*(4), 363–380.

Berliand, M. E. (1952). Determining the net long-wave radiation of the earth with consideration of the effect of cloudiness. *Izvestiya Akademii Nauk SSSR, Seriya Geologicheskaya*, *1*, 64–78.

Bernie, D. J., Guilyardi, E., Madec, G., Slingo, J. M., Woolnough, S. J., Bernie, D. J., . . . Woolnough, S. J. (2007). Impact of resolving the diurnal cycle in an ocean–atmosphere GCM. Part 1: A diurnally forced OGCM. *Climate Dynamics*, *29*(6), 575–590.

Bernie, D. J., Woolnough, S. J., Slingo, J. M., & Guilyardi, E. (2005). Modeling diurnal and intraseasonal variability of the ocean mixed layer. *Journal of Climate*, *18*(8), 1190–1202.

Boyer, T., Levitus, S., Garcia, H., Locarnini, R. A., Stephens, C., & Antonov, J. (2005). Objective analyses of annual, seasonal, and monthly temperature and salinity for the World Ocean on a 0.25° grid. *International Journal of Climatology*, *25*(7), 931–945.

Carton, J. A., Chepurin, G., & Cao, X. (2000). A simple ocean data assimilation analysis of the global upper ocean 1950 95. Part II: Results. *Journal of Physical Oceanography*, *30*(30), 311–326.

Carton, J. A., & Giese, B. S. (2008). A Reanalysis of ocean climate using Simple Ocean Data Assimilation (SODA). *Monthly Weather Review*, *136*(136), 2999.

Chapman, D. C. (1985). Numerical treatment of cross-shelf open boundaries in a barotropic coastal ocean model. *Journal of Physical Oceanography*, *15*(15), 1060–1075.

Clayson, C. A., & Weitlich, D. (2005). Diurnal warming in the tropical Pacific and its interannual variability. *Geophysical Research Letters*, *32*, L21604. https://doi.org/10.1029/2005GL023786

Cornillon, P., & Stramma, L. (1985). The distribution of diurnal sea surface warming events in the western Sargasso Sea. *Journal of Geophysical Research*, *901*(C6), 11811–11816.

Donlon, C. J., Martin, M., Stark, J., Roberts-Jones, J., Fiedler, E., & Wimmer, W. (2012). The Operational Sea Surface Temperature and Sea Ice Analysis (OSTIA) system. *Remote Sensing Environment*, *116*(2), 140–158.

Egbert, G. D., Bennett, A. F., & Foreman, M. G. G. (1995). TOPEX/Poseidon tides estimated using a global inverse model. *Journal of Geophysical Research*, *99*(C12), 24821–24852.

Egbert, G. D., & Erofeeva, S. Y. (2002). Efficient inverse modeling of barotropic ocean tides. *Journal of Atmospheric Oceanic Technology*, *19*(2), 183–204.

Fairall, C. W., Bradley, E. F., Hare, J. E., Grachev, A. A., & Edson, J. B. (2003). Bulk parameterization of air sea fluxes: Updates and verification for the COARE Algorithm. *Journal of Climate*, *16*(4), 571–591.

Fairall, C. W., Bradley, E. F., Rogers, D. P., Edson, J. B., & Young, G. S. (1996a). Bulk parameterization of air-sea fluxes for Tropical Ocean-Global Atmosphere Coupled-Ocean Atmosphere Response Experiment. *Journal of Geophysical Research*, *101*(C2), 3747–3764.

Fairall, C. W., Godfrey, J. S., Bradley, E. F., Wick, G. A., Edson, J. B., & Young, G. S. (1996b). Cool-skin and warm-layer effects on sea surface temperature. *Journal of Geophysical Research*, *101(C1)*, 1295–1308. https://doi.org/10.1029/95JC03190

Fasullo, J., & Webster, P. J. (2000). Atmospheric and surface variations during westerly wind bursts in the tropical western pacific. *Quarterly Journal of the Royal Meteorological Society*, *126*(564), 899–924.

Fei, Y. U., Zhang, Z. X., Lan, J., Diao, X. Y., Guo, J. S., & Reng Feng, G. E. (2005). Analysis of water temperature distribution characteristics in the southern Yellow Sea in Spring. *Advances in Marine Sciences*, *23*(3), 281–288.

Flament, P., Firing, J., Sawyer, M., & Trefois, C. (1994). Amplitude and horizontal structure of a large diurnal sea surface warming event during the coastal ocean dynamics experiment. *Journal of Physical Oceanography*, *24*(1), 124–139.

Flather, R. A. (1976). A tidal model of northwest European continental shelf. *Memoires Societe Royale des Sciences de Liege*, *10*, 141–164.

Gentemann, C. L., Minnett, P. J., & Ward, B. (2009). Profiles of ocean surface heating (POSH): A new model of upper ocean diurnal warming. *Journal of Geophysical Research*, *114*, C07017. https://doi.org/10.1029/2008JC004825

Gill, A. E. (1982). *Atmosphere-ocean dynamics*. Cambridge, MA: Academic Press.

Gille, S. T. (2012). Diurnal variability of upper ocean temperatures from microwave satellite measurements and Argo profiles. *Journal of Geophysical Research*, *117*, C11027. https://doi.org/10.1029/2012JC007883

Guemas, V., Salasmélia, D., Kageyama, M., Giordani, H., & Voldoire, A. (2011). Impact of the ocean diurnal variations on the intraseasonal variability of Sea Surface Temperatures in the Atlantic Ocean. *Journal of Climate*, *24*(12), 845–853.

Hyder, P., Simpson, J. H., Xing, J., & Gille, S. T. (2011). Observations over an annual cycle and simulations of wind-forced oscillations near the critical latitude for diurnal–inertial resonance. *Continental Shelf Research*, *31*, 1576–1591.

Kahru, M., Leppanen, J. M., & Rud, O. (1993). Cyanobacterial blooms cause heating of the sea surface. *Marine Ecology Progress Series*, *101*(1–2), 1–8. https://doi.org/10.3354/meps101001

Kalnay, E., Kanamitsu, M., Kistler, R., Collins, W., Deaven, D., Gandin, L., . . . Woollen, J. (1996). The NCEP/NCAR 40-Year Reanalysis Project. *Bulletin of American Meteorological Society*, *77*(3), 437–472.

Katsaros, K. B., Soloviev, A. V., Weisberg, R. H., & Luther, M. E. (2005). Reduced horizontal sea surface temperature gradients under conditions of clear skies and weak winds. *Boundary-Layer Meteorology*, *116*(2), 175–185. https://doi.org/10.1007/s10546-004-2421-4

Kawai, Y., & Kawamura, H. (2005). Spatial and temporal variations of model-derived diurnal amplitude of sea surface temperature in the western Pacific Ocean. *Journal of Geophysical Research*, *110*, C08012. https://doi.org/10.1029/2004JC002652

Kawai, Y., & Wada, A. (2007). Diurnal sea surface temperature variation and its impact on the atmosphere and ocean: A review. *Journal of Oceanography*, *63*(5), 721–744.

Kettle, H., Merchant, C. J., Jeffery, C. D., Filipiak, M. J., & Gentemann, C. L. (2009). The impact of diurnal variability in sea surface temperature on the central Atlantic air-sea CO2 flux. *Atmospheric Chemistry and Physics*, *8*(2), 529–541.

Lau, K. M., & Sui, C. H. (2010). Mechanisms of short-term sea surface temperature regulation: Observations during TOGA COARE. *Journal of Climate*, *10*(3), 465–472.

Lee, T., & Liu, W. T. (2005). Effects of high-frequency wind sampling on simulated mixed layer depth and upper ocean temperature. *Journal of Geophysical Research*, *110*, C05002. https://doi.org/10.1029/2004JC002746

Li, J., Li, G., Xu, J., Dong, P., Qiao, L., Liu, S., Sun, P., & Fan, Z. (2016). Seasonal evolution of the Yellow Sea Cold Water Mass and its interactions with ambient hydrodynamic system. *Journal of Geophysical Research: Oceans*, *121*, 6779–6792. https://doi.org/10.1002/2016JC012186

Li, Y., Han, W., Shinoda, T., Wang, C., Lien, R. C., Moum, J. N., & Wang, J. W. (2013). Effects of the diurnal cycle in solar radiation on the tropical Indian Ocean mixed layer variability during wintertime Madden-Julian Oscillations. *Journal of Geophysical Research: Oceans*, *118*, 4945–4964. https://doi.org/10.1002/jgrc.20395

Locarnini, A. R., Mishonov, A. V., Antonov, J. I., Boyer, T. P., Garcia, H. E., Baranova, O. K., . . . Reagan, J. R. (2013). Volume 1: Temperature. In S. Levitus (Ed.), *NOAA Atlas NESDIS 73 World Ocean Atlas 2013*. Washington, DC: U.S. Government Printing Office.

McCreary, P., Kohler, K. E., Hood, P., John, S., Albert, K., & Fischer, S. (2001). Influences of diurnal and intraseasonal forcing on mixed-layer and biological variability in the central Arabian Sea. *106*(C4), 7139–7155.

Mellor, G. L., & Yamada, T. (1982). Development of a Turbulent Closure Model for Geophysical Fluid Problems. *Review of Geophysics*, *20*(4), 851–875.

Merchant, C. J., Filipiak, M. J., Le Borgne, P., Roquet, H., Autret, E., Piollé, J.-F., & Lavender, S. (2008). Diurnal warm-layer events in the western Mediterranean and European shelf seas. *Geophysical Research Letters*, *35*, L04601. https://doi.org/10.1029/2007GL033071

Orlanski, I. (1976). A simple boundary condition for unbounded hyperbolic flows. *Journal of Computational Physics*, *21*(3), 251–269.

Paulson, C. A., & Simpson, J. J. (1977). Irradiance measurements in the upper ocean. *Journal of Physical Oceanography*, *7*, 953–956.

Price, J. F., Weller, R. A., Bowers, C. M., & Briscoe, M. G. (1987). Diurnal response of sea surface temperature observed at the long-term upper ocean study (34°N, 70°W) in the Sargasso Sea. *Journal of Geophysical Research*, *92*(C13), 14480–14490.

Price, J. F., Weller, R. A., & Pinkel, R. (1986). Diurnal cycling: Observations and models of the upper ocean response to diurnal heating, cooling, and wind mixing. *Journal of Geophysical Research*, *91*(C7), 8411–8427.

Qiao, F., Yuan, Y., Yang, Y., Zheng, Q., Xia, C., & Ma, J. (2004). Wave-induced mixing in the upper ocean: Distribution and application to a global ocean circulation model. *Geophysical Research Letters*, *31*, L11303. https://doi.org/10.1029/2004GL019824

Quan, Q., Mao, X., Yang, X., Yingying, H. U., Zhang, H., & Jiang, W. (2013). Seasonal variations of several main water masses in the southern Yellow Sea and East China Sea in 2011. *Journal of Ocean University of China*, *12*(4), 524–536.

Saha, S., Moorthi, S., Pan, H. L., Wu, X. R., Wang, J. D., Nadiga, S., . . . Behringer, D. (2010). The NCEP climate forecast system reanalysis. *Bulletin of American Meteorological Society*, *91*(8), 1015–1057.

Sakaida, F., Kudoh, J. I., & Kawamura, H. (2000). A-HIGHERS—The system to produce the high spatial resolution sea surface temperature maps of the western North Pacific using the AVHRR/NOAA. *Journal of Oceanography*, *56*(6), 707–716.

Schiller, A., & Godfrey, J. S. (2005). A diagnostic model of the diurnal cycle of sea surface temperature for use in coupled ocean-atmosphere models. *Journal of Geophysical Research*, *110*, C11014. https://doi.org/10.1029/2005JC002975

Shchepetkin, A. F., & Mcwilliams, J. C. (2005). The regional oceanic modeling system (ROMS): A split-explicit, free-surface, topography-following-coordinate oceanic model. *Ocean Modelling*, *9*(4), 347–404.

Shchepetkin, A. F., & Mcwilliams, J. C. (2009). Correction and commentary for "Ocean forecasting in terrain-following coordinates: Formulation and skill assessment of the regional ocean modeling system" by Haidvogel et al., J. Comp. Phys. 227, pp. 3595–3624. *Journal of Computational Physics*, *228*(24), 8985–9000.

Simpson, J. H., & Bowers, D. (1981). Models of stratification and frontal movement in shelf seas. *Deep Sea Research Part A: Oceanographic Research Papers*, *28*(7), 727–738.

Solomon, A., & Jin, F. F. (2005). A study of the impact of off-equatorial warm pool SST anomalies on ENSO cycles. *Journal of Climate*, *18*(2), 274–286.

Stramma, L., Cornillon, P., Weller, R. A., Price, J. F., & Briscoe, M. G. (1986). Large Diurnal sea surface temperature variability: Satellite and in situ measurements. *Journal of Physical Oceanography*, *16*(5), 827–837.

Thomson, R. E., & Fine, I. V. (2003). Estimating mixed layer depth from oceanic profile data. *Journal of Atmospheric Ocean. Technology*, *20*(20), 319.

Vialard, J., Shenoi, S. S. C., Mccreary, J. P., Shankar, D., Durand, F., Fernando, V., & Shetye, S. R. (2009). Intraseasonal response of the northern Indian Ocean coastal waveguide to the Madden-Julian Oscillation. *Geophysical Research Letters*, *36*, L14606. https://doi.org/10.1029/2009GL038450

Vorosmarty, C. J., Fekete, B. M., & Tucker, B. A. (1998). Global River Discharge, 1807–1991, V[ersion]. 1.1 (RivDIS). Data set. Oak Ridge, TN: Oak Ridge National Laboratory Distributed Active Archive Center. Retrieved form http://www.daac.ornl.gov; https://doi.org/10.3334/ORNLDAAC/199

Ward, B. (2006). Near-surface ocean temperature. *Journal of Geophysical Research*, *111*, C02005. https://doi.org/10.1029/2004JC002689

Ward, B., Wanninkhof, R., Mcgillis, W. R., Jessup, A. T., Degrandpre, M. D., Hare, J. E., & Edson, J. B. (2004). Biases in the air-sea flux of CO 2 resulting from ocean surface temperature gradients. *Journal of Geophysical Research*, *109*, C08S08. https://doi.org/10.1029/2003JC001800

Webster, P. J., Clayson, C. A., & Curry, J. A. (1996). Clouds, radiation, and the diurnal cycle of sea surface temperature in the tropical Western Pacific. *Journal of Climate*, *9*(8), 1712–1730.

Webster, P. J., Magaña, V. O., Palmer, T. N., Shukla, J., Tomas, R. A., Yanai, M., & Yasunari, T. (1998). Monsoons: Processes, predictability, and the prospects for prediction. *Journal of Geophysical Research*, *1031*(C7), 14451–14510.

Wei, W., Xinhua, F., & Dexing, W. (2001). On the methods of determining the depths of thermocline, halocline and pycnocline. *Transactions of Oceanology and Limnology*, *2*, 0001–0007. https://doi.org/10.13984/j.cnki.cn37-1141.2001.02.001

Xia, C., Qiao, F., Yang, Y., Ma, J., & Yuan, Y. (2006). Three-dimensional structure of the summertime circulation in the Yellow Sea from a wave-tide-circulation coupled model. *Journal of Geophysical Research*, *111*, C11S03. https://doi.org/10.1029/2005JC003218

Yokoyama, R., Tanba, S., & Souma, T. (1995). Sea surface effects on the sea surface temperature estimation by remote sensing. *International Journal of Remote Sensing*, *16*(2), 227–238.

Yu, Y., Gao, H., & Shi, J. (2017). Impacts of diurnal forcing on temperature simulation in the shelf seas of China [in Chinese with English abstract and figure caption]. *Periodical of Ocean University of China*, *47*(4), 106–113. Retrieved from http://oversea.cnki.net/kcms/detail/detail.aspx?recid=&FileName=QDHY201704015&DbName=CJF. https://doi.org/10.16441/j.cnki.hdxb.20160138

Zeng, X., & Dickinson, R. E. (1998). Impact of diurnally-varying skin temperature on surface fluxes over the tropical Pacific. *Geophysical Research Letters*, *25*(9), 1411–1414.

Zhang, S. W., Wang, Q. Y., Lü, Y., Cui, H., & Yuan, Y. L. (2008). Observation of the seasonal evolution of the Yellow Sea Cold Water Mass in 1996–1998. *Continental Shelf Research*, *28*(3), 442–457.

Zweng, M. M., Reagan, J. R., Antonov, J. I., Locarnini, R. A., Mishonov, A. V., Boyer, T. P., . . . Johnson, D. R. (2013). Volume 2: Salinity. In *World Ocean Atlas 2013* (*NOAA Atlas NESDIS 74*).